ORIGINAL ARTICLE   OPEN

The cellular landscape of the endochondral bone during the transition to extrauterine life

Alejandro Díaz Rueda[1,a] (iD), Irepan Salvador-Martínez[2,a] (iD), Ismael Sospedra-Arrufat[1] (iD), Ana Alcaina-Caro[1] (iD), Ana Fernández-Miñán[1] (iD), Ana M Burgos-Ruiz[1], Ildefonso Cases[1] (iD), Alberto Mohedano[3] (iD), Juan J Tena[1] (iD), Holger Heyn[2] (iD), Javier Lopez-Rios[1,4] (iD) 🐦 & Gretel Nusspaumer[1] (iD)

1 Centro Andaluz de Biología del Desarrollo (CABD), CSIC-Universidad Pablo de Olavide-Junta de Andalucía, Seville, Spain
2 CNAG-CRG, Centre for Genomic Regulation (CRG), Barcelona Institute of Science and Technology (BIST), Barcelona, Spain
3 Intensive Care Unit, Severo Ochoa University Hospital Leganés, Madrid, Spain
4 Universidad Loyola Andalucía, School of Health Sciences, Dos Hermanas, Seville, Spain

Review COMMONS

Abstract

The cellular complexity of the endochondral bone underlies its essential and pleiotropic roles during organismal life. While the adult bone has received significant attention, we still lack a deep understanding of the perinatal bone cellulome. Here, we have profiled the full composition of the murine endochondral bone at the single-cell level during the transition from fetal to newborn life and in comparison with the adult tissue, with particular emphasis on the mesenchymal compartment. The perinatal bone contains different fibroblastic clusters with blastema-like characteristics in organizing and supporting skeletogenesis, angiogenesis and hematopoiesis. Our data also suggest dynamic inter- and intra-compartment interactions, as well as a bone marrow milieu that seems prone to anti-inflammation, which we hypothesize is necessary to ensure the proper program of lymphopoiesis and the establishment of central and peripheral tolerance in early life. Our study provides an integrative roadmap for the future design of genetic and cellular functional assays to validate cellular interactions and lineage relationships within the perinatal bone.

INTRODUCTION

Important changes take place during the transition from intrauterine to extrauterine life. The newborn is deprived of nutrients, heat, and the buoyant and pathogen-protected environment of the womb. Among other major organismal changes, the lungs inflate and the cardiovascular flow is adjusted as the newborn begins to breathe. High hormonal levels are present in preparation

for the sharp increase in the metabolic rate and thermoregulation. Brown fat tissue, accumulated during late gestation, plays an important metabolic and thermal role during the first days of life. The increased mechanical load and movement impacts on the skeleton of the newborn, where the osteogenic program will also be affected by the rise in oxygen supply. The establishment of the intestinal microbiome and its crosstalk with the still immature immune system will also

impact on the program of hematopoiesis in the bone marrow which started at late fetal stages.[1,2] The skeleton has a pivotal position in many of these processes, given its roles in body support, movement, organ protection, hematopoiesis and hormonal and metabolic control.

Endochondral bone-derived mesenchymal progenitors are capable of engaging in chondrogenic, osteogenic and adipogenic differentiation programs, and give rise to specialized bone marrow stromal cells (BMSC) that support hematopoiesis.[3] The development of long bones is a dynamic and tightly orchestrated process, reflecting the capacity of mesenchymal progenitors to first generate cartilage, which serves as a mold and provides the signals to initiate the program of osteogenesis and the formation of bone marrow (BM).[4,5] During the formation of the bone marrow, some mesenchymal progenitors remain as BMSC, supporting hematopoiesis, while also retaining the capacity to differentiate into osteoblasts and adipocytes.[6,7] Genetic cell-fate tracking, prospective immunophenotype characterization, and, more recently, scRNAseq studies in mice are revealing the complex nature of the bone mesenchymal compartment, as well as the versatility of its different cell populations and their division of labor.[8] For example, the capacity of hypertrophic chondrocytes to transdifferentiate into osteoblasts is now well accepted in the field.[9,10] Moreover, bone fracture and fingertip regeneration models in mice, along with studies on limb regeneration in other vertebrates, are challenging ingrained concepts and point to alternative models by which different populations (e.g. fibroblastic cells) can be recruited and reprogrammed in a highly plastic fashion, including cellular phenotypic convergence.[6,9,11–14] However, most of these studies have focused on adult bone, and we still lack fundamental knowledge about the heterogeneity, relationships and interactions between the mesenchymal and hematopoietic compartments at perinatal stages. To capture the main key features of these processes, we have generated a comprehensive scRNA-seq cellular map of all mouse endochondral bone compartments just before and after birth (E18.5 and postnatal day [PN] 1). The analysis of these datasets, in comparison with those from adult mice,[15] shows that the composition and molecular fingerprint of several bone populations change significantly between these stages. Of note, our resource study reveals the presence of distinct perinatal fibroblastic mesenchymal populations with molecular signatures that suggest their involvement in the formation of the bone marrow, organization of angiogenesis and peripheral innervation, as well as in establishing the environment for proper hematopoiesis, including potential direct interactions between specific mesenchymal and hematopoietic clusters. Our study also identifies mesenchymal clusters with active immunomodulatory transcriptional programs, which may be involved in setting an anti-inflammatory setup with implications for the maturation of the immune system and the self from non-self discrimination that is just starting to take shape. Overall, our findings underscore the relevance of integrative ontogenic studies that take into account the full cellular complexity of endochondral bone and have important implications for the prospective isolation of cell populations for tissue engineering applications as well as for the age-tailoring of disease treatments.

RESULTS

A cell atlas of the perinatal endochondral bone

To gain a comprehensive understanding of the composition and dynamics of endochondral bone during the transition from intrauterine to extrauterine life, with particular emphasis on the mesenchymal compartment, we adopted a FACS-enrichment strategy that ensured that all cellular components of the E18.5 and PN1 endochondral bone (forelimbs, excluding the autopod) could be captured by scRNA-seq in a balanced manner. This strategy is similar to that previously used for adult bone,[15] and allows the investigation of not only the relationships between mesenchymal subpopulations, but also their involvement in angiogenesis, hematopoiesis and peripheral nervous system development. To represent both abundant and scarce populations, we employed the sorting strategy depicted in Figure 1a (see Methods). Briefly, dead cells and multiplets were excluded by gating, and lineage labeling was avoided to prevent the loss of any cell subsets. The gates were defined by the use of a mix of pan-antibodies targeting mesenchymal (CD140a/PDGFR-a) and endothelial cells (CD31/PECAM), as well as CD9, a marker highly expressed in early hematopoietic progenitors and stromal cells (nicheview.shiny.embl.de[15]). Sorted cells were mixed in different proportions to better represent less abundant populations (Figure 1a). Although this strategy is not quantitative, it enables the monitoring of relative changes in cell numbers between equivalent clusters at both stages. After quality control, 7272 (E18.5) and 7277 (PN1) high-quality cells were recovered for analysis, averaging 2625 and 2533 genes per cell, respectively.

A combination of unsupervised and curated clustering resulted in the identification of 24 cell populations, each characterized by a distinct molecular signature (Figure 1b, c, Supplementary figures 1 and 2). These clusters encompass all hematopoietic, mesenchymal and endothelial compartments in the perinatal endochondral bone. The entire hematopoietic compartment (HC, encircled in dark blue)

Figure 1. A cell atlas of the perinatal endochondral bone. **(a)** Gating strategy used for processing of cell suspensions for scRNA-seq, obtained after enzymatic digestion of forelimb long bones at E18.5 and PN1 (see Methods for details). The number of sorted cells that were mixed for each gate is indicated by the color codes used in the flow cytometry (FC) pseudocolor plots. **(b)** Uniform Manifold Approximation and Projection (UMAP) of annotated clusters at E18.5 and PN1 after Harmony integration. Mesenchymal cells (MC) are encircled in green, hematopoietic cells (HC) in dark blue, endothelial cells (EC) in magenta and Schwann cells (SC) in turquoise. ACP, articular cartilage population; AFP, adipose fibroblastic population; B Lin, B-cell lineage; ChC, chondrogenic cells; CLFP, *Cxcl12*-low fibroblastic population; Eo Bas, eosinophils and basophils; Ery, erythrocytes; GFP, *Gas6*$^+$ fibroblastic population; HPC, hematopoietic progenitor cells; ILC_TSP2, innate lymphoid cells and thymic seeding progenitors 2; Im Neu, immature neutrophils; Mon DC, monocytes and dendritic cells; Myo, myofibroblasts; Neu, neutrophils; Oc, osteoclasts; OsC, osteogenic cells; PFP, proliferating fibroblastic population; PHP, proliferating hematopoietic progenitors; SC, Schwann cells; Sca1 HC, Sca-1$^+$ hematopoietic cells; SFP, Sca-1$^+$ fibroblastic population; TC, tenogenic cells. **(c)** Dotplot of representative genes across perinatal (E18.5 and PN1) clusters. Dot color and size indicate the average expression levels and the percentage of cells within a cluster that express the selected gene, respectively. Gene expression is normalized and scaled relative to the entire dataset (mean = 0; s.d. = 1), so negative values correspond to expression levels that are lower than the global mean expression. **(d)** Stacked-bar charts indicating the proportions of cells assigned to each cluster at E18.5 and PN1.

and its constituent clusters are distinguished by the expression of defining markers such as *Ptprc* (pan-HC), *Cd79a* (B-Lin), *CD200r3* (Eo-Bas) and so on. Recent scRNAseq, scATAC and scProteo-genomic studies have demonstrated that FACS-isolated oligopotent progenitors represent heterogeneous mixtures of progenitor populations.[16,17] As they were not our primary focus, we opted for broad categories for the definition of HC clusters. For example, HPC (hematopoietic progenitor cells) encompasses granulocyte/monocyte progenitors, megakaryocyte progenitors and LMPP (lymphoid myeloid primed progenitors); likewise, the B-Lin cluster includes all stages of B cell maturation. The endothelial compartment is

represented by a single cluster (EC; encircled in purple in Figure 1b), defined by the expression of pan-endothelial genes such as *Cdh5* or *Pecam1*/CD31.

Within the mesenchymal compartment (MC; encircled in light green), clusters representing fate-committed progenitors or differentiated cells were readily identified based on their molecular signature (Figure 1b, c, Supplementary figures 1 and 2). The chondrogenic (ChC) cluster was defined by the expression of the *Sox9*/*Sox5*/*Sox6* trio, which drives the transcription of *Col2a1*, *Acan*, *Col9a1*, *Col9a2* and *Col9a3*.[18] The osteogenic (OsC) cluster was distinguished by the expression of *Runx2*, *Osterix*/Sp7, *Bglap*/Osteocalcin, *Spp1*/Osteonectin and *Isbp*/bone

sialoprotein.[19] Finally, the myofibroblast (Myo) cluster was characterized by the expression of key myogenic genes such as *Pax7, Myf5, Msc, Myod1* and *Acta2/aSMA*.[20] In addition, we defined seven closely associated clusters of fibroblastic nature. These included a cell population with tenogenic characteristics (TC),[21–23] expressing *Scx*/Scleraxis, *Tnmd*/Tenomodulin, *Kera*/Keratocan and *Cpxm2*, as well as an articular cartilage progenitor (ACP) cluster expressing *Sox5, Gdf5, Pthlh, Barx1, Prg4* and *Wnt4* (Figure 1c, Supplementary figures 1 and 2).[24,25] We also identified *Tspan15* and *Ackr2* as novel ACP markers, with implications in bone growth and remodeling.[26,27] The remaining five mesenchymal clusters were even closer in the UMAP space and annotated as GFP (*Gas6*⁺ fibroblastic population, also enriched in *Eln*-expressing cells), SFP (Sca-1/*Ly6a*⁺ fibroblastic population, expressing other markers such as *Ly6c1*), AFP (adipogenic fibroblastic population, expressing *Ptch2* and *Notch3*), CLFP (*Cxcl12*-low fibroblastic population, expressing *Ly6h* and *Lpl*) and PFP (proliferating fibroblastic population; Figure 1c, Supplementary figures 1 and 2). The PFP population comprises cells in S or G2/M phases of the cell cycle and expresses mitogenic genes such as *Mki67, Nusap1, Cenpe* and *Ccna2* (Figure 1c, Supplementary figures 1 and 2). PFP includes the proliferating fractions of the GFP, SFP, AFP and CLFP clusters, but only a minimal part of ACP cells, which fits the long-lasting quiescency of articular progenitors.[28] Cell-cycle analysis also revealed small proliferating subsets within other hematopoietic and mesenchymal clusters, including ChC and Myo (Supplementary figure 2b, c). The comparison of cluster ratios indicated changes in both hematopoietic and mesenchymal compartments during the transition to extrauterine life, including a notable increase in the representation of SFP, AFP and TC clusters at PN1 when compared with E18.5 (Figure 1d). Since each sample per stage was obtained by pooling littermate tissue from both sexes, we deconvoluted the scRNA-seq datasets according to the expression of sex-specific genes. All clusters identified in the pooled samples were present in both females and males and the trends observed in the SFP, AFP and TC clusters between E18.5 and PN1 were maintained (Supplementary figure 3). In light of these results, all downstream analyses were performed using the pooled samples.

Highlighting the differences between perinatal and adult bone mesenchymal compartments

Next, we used Harmony[29] to integrate our perinatal scRNA-seq datasets with those reported previously for adult mice,[15] which were generated from femurs, tibiae, hips and spines from 8- to 12-week-old females (Figure 2, Supplementary figures 4 and 5). This analysis revealed a broad correlation between both stages, with related clusters falling into equivalent positions within the integrated UMAP space, except for PFP, which was disconnected from the main fibroblastic clusters and split into three components (asterisks in Figure 2a). Cell cycle analysis indicated that, in contrast to perinatal stages where all compartments are proliferating, only the adult hematopoietic compartment displays cells in S and G2/M phases (Figure 2b). Focusing on the mesenchymal compartment, adult chondrocytes and myofibroblasts had perinatal counterparts. The closely associated SFP, GFP, AFP and CLFP perinatal clusters were located in similar UMAP coordinates as the adult endosteal, arteriolar and stromal fibroblasts, while perinatal ACP and TC were not clearly identified in the adult scRNAseq dataset (see Discussion).

One of the most studied bone mesenchymal populations are CARs (*Cxcl12*-abundant reticular cells[30]), and seminal studies over the past decade have identified their pivotal role in hematopoiesis. CARs are also characterized by the expression of *Kitl* and constitute almost all *Lepr*-expressing cells (Figure 2c).[31] scRNAseq studies have further subdivided CARs based on their adipogenic (*Cxcl12*⁺, *Alpl*^meg) or osteogenic profiles (*Cxcl12*⁺, *Alpl*⁺)[15,32] and identified even more subsets,[33–35] reflecting their adipogenic, osteogenic and BMSC differentiation potential. The comparison between equivalent UMAP plot coordinates at perinatal and adult stages (boxed area in Figure 2c) revealed an almost complete absence of AdipoCARs in perinatal bone, and markers highly detected in adult Adipo-CARs (*Lepr, Cxcl12, Kitl, Pparg, Adipoq* and *Vcam1*/CD106)[6,36] were expressed in very few cells at perinatal stages, adjacent to the OsC cluster (Figure 2c). These results suggest that Adipo-CARs are just beginning to emerge at perinatal stages and are in keeping with other reports using LepR antibodies, *Lepr*-CreER lines induced in early postnatal life, and recent scRNAseq analysis of the stromal compartment at postnatal day 4.[7,37,38] Of note, *Cxcl12, Kitl, Gas6* and *Lpl* were all expressed at lower levels in fibroblastic clusters, primarily in CLFP, AFP and GFP (Figure 2c and Supplementary figure 4), suggesting the possibility that some Adipo-CAR progenitors could be contained within these clusters. In line with this hypothesis, *Pparg* and *LepR*, key factors in the adipogenic program that starts to shape perinatally, are expressed in a scattered manner in the perinatal fibroblastic clusters, including AFP cells (Figure 2c and Supplementary figure 4). In contrast, there is a good correlation between the perinatal OsC cluster and adult osteogenic cells, which include Osteo-CARs, Ng2⁺ cells and osteoblasts, with high expression of osteogenic genes (Figure 2c and Supplementary figure 4). As others have described for adult bone,[15,39,40] we also located the perinatal prospective mSSC (murine Skeletal Stem Cells,[41] characterized by the
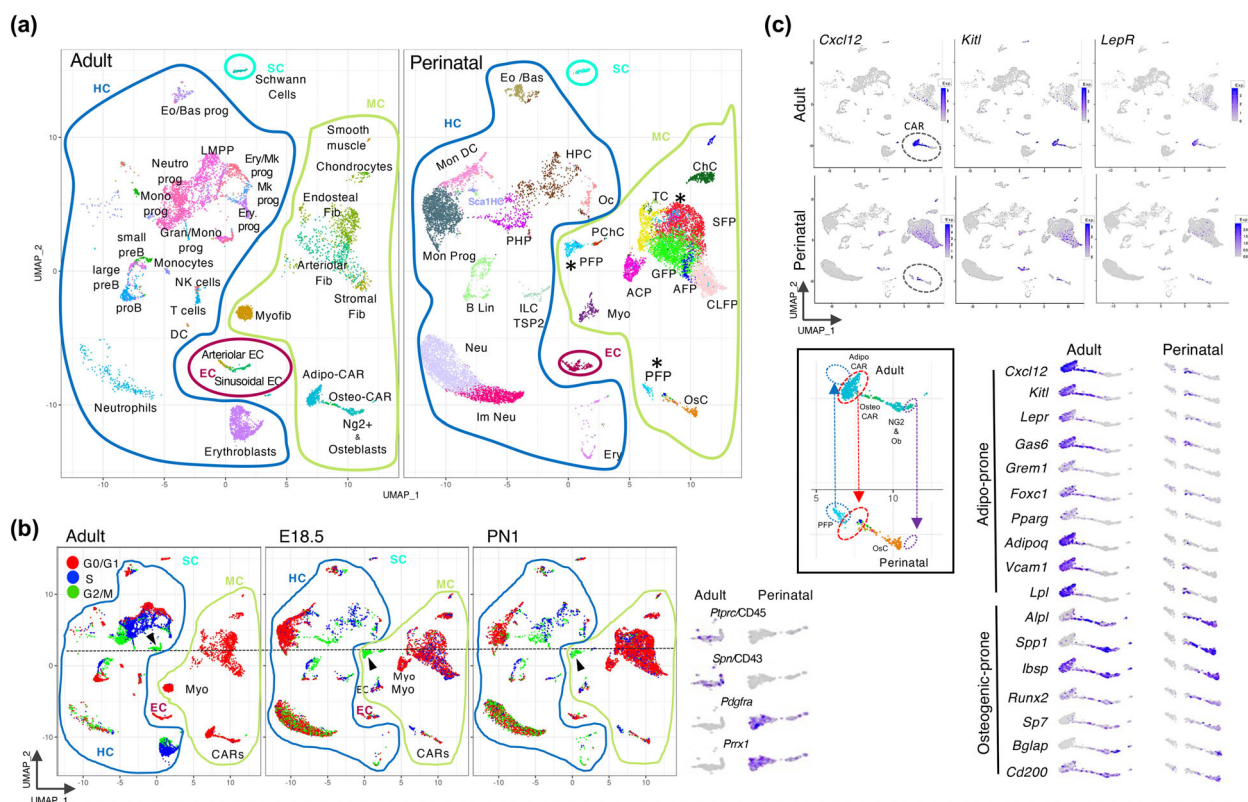
Figure 2. Differences between perinatal and adult bone. **(a)** UMAP plot of Harmony-integrated adult[15] and perinatal scRNAseq datasets. Note that the integration with adult data alters the distribution of clusters in comparison with Figure 1 (e.g. PFP, indicated by asterisks). PChC, proliferating chondrogenic cells; PFP, proliferating fibroblastic population. **(b)** Cell cycle analysis of the Harmony-integrated adult and perinatal scRNAseq datasets. Arrowheads and dotted lines indicate G2/M clusters that correspond to adult HC ($Ptprc^+$ and Spn^+) and that in perinatal stages are part of the PFP mesenchymal cluster (positive for $Pdgfra^+$ and $Prrx1^+$). **(c)** Genes expressed in adult CARs and their expression at perinatal stages (upper panels). Lower left box: enlarged view to visualize the coordinates of AdipoCARs in adult and their absence in perinatal stages. Lower right panel: magnification of CAR clusters and overlay of adult Adipo- and Osteo-CARs markers with the cellular map of perinatal bone.

immunophenotype CD51$^+$ CD200$^+$; negative for CD45, CD31 and TER119, CD90, CD105, 6C3; Supplementary figure 5a) in the osteogenic-related OsC cluster. The integral analysis of all bone cell populations (Baccin *et al.*[15] and this study) also unveils, with high resolution, the specific and temporal (perinatal *versus* adult) expression patterns of reported genetic drivers and surface marker-encoding genes, providing a valuable resource for the interpretation of previous observations using cell-fate tracing mouse models and prospective isolation strategies (Supplementary figure 5). A major advantage of including all endochondral bone populations in scRNA-seq experiments is that it provides a rich resource for identifying markers whose expression is restricted to specific populations. To illustrate this, we identified various genes that are preferentially expressed in the different perinatal fibroblastic clusters, which will allow the design of more precise inducible genetic tools (Supplementary

figure 6). Emphasizing the relevance of performing ontogenic studies, we identified genes active at perinatal stages that are not expressed in the adult tissue.

In-depth analysis of the mesenchymal compartment

Next, we generated a new Harmony representation focused solely on the mesenchymal clusters to more effectively illustrate their relationships at E18.5 and PN1 (Figure 3a). As noted previously, we observed an increase in SFP and TC populations after birth. In the case of the TC population (labeled by *Scx* and *Tnmd* expression), two distinct branches were identified. One branch is related to the chondrogenic cluster, while the other likely represents tenogenic precursors, as it is preferentially labeled by additional tendon markers such as *Mkx* and *Kera* (Figure 3b). This branch is also highly specifically labeled by *Ptx4*, making this locus a good candidate for
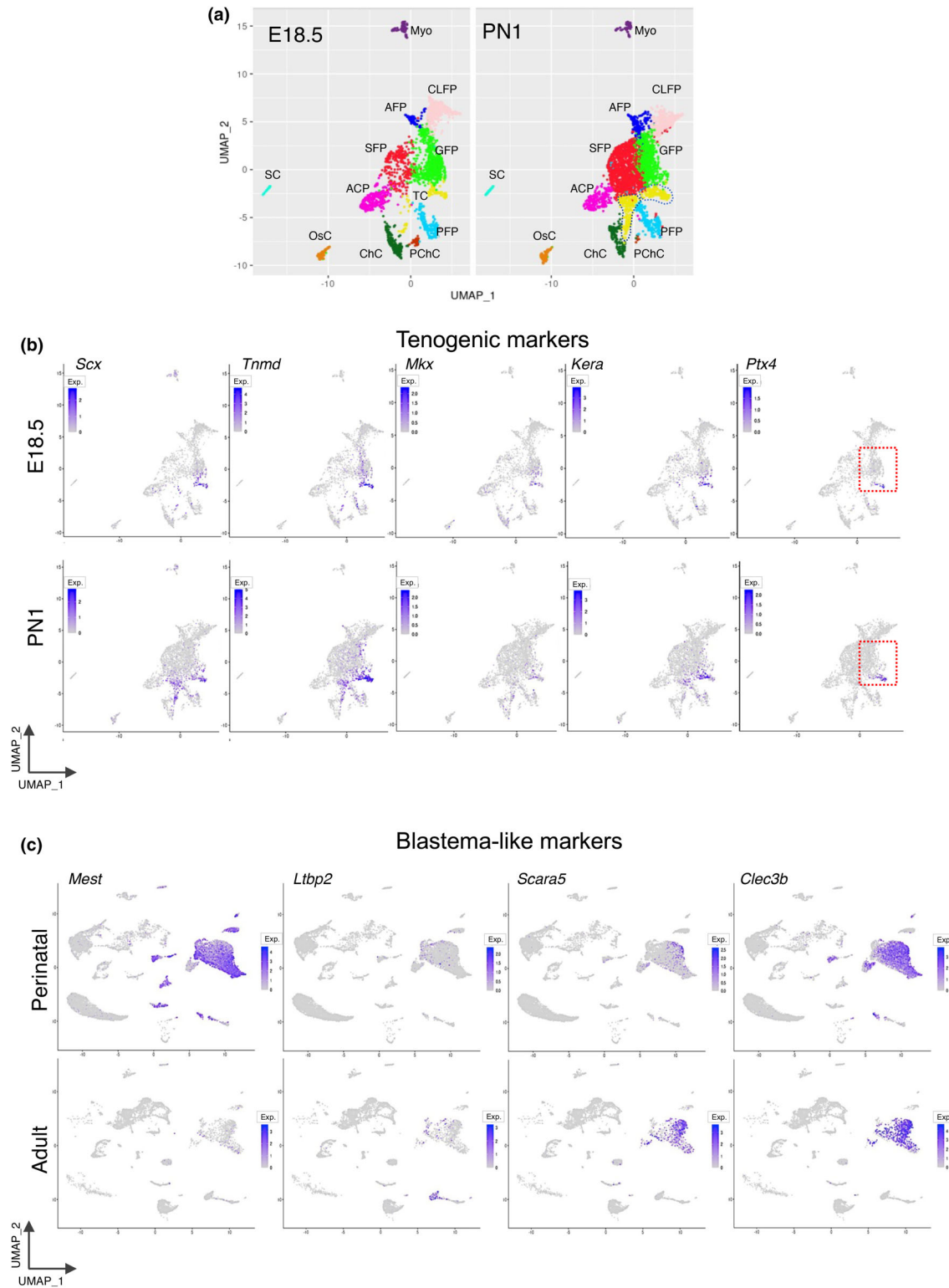
Figure 3. Hierarchy between mesenchymal clusters of the perinatal bone. **(a)** Harmony integration of mesenchymal clusters at E18.5 and PN1. The two branches of the TC cluster at PN1 are labeled by a dotted line. **(b)** Expression of TC-specific genes at E18.5 and PN1. *Ptx4* is exclusively expressed in the tenogenic branch (red box). **(c)** Expression in perinatal and adult bone of genes identified in dermal and blastema cells in the mouse digit tip regeneration model.

the design of genetic tools to study tendon development and regeneration.

To gain insight into the closely connected GFP, SFP, AFP and CLFP clusters, we conducted Gene Ontology (GO) analyses based on their differentially expressed genes E18.5 and PN1 (gene number ranging between 185 and 480; Supplementary table 1 and Supplementary figure 7). These results associated CLFP, GFP and SFP with extracellular matrix (ECM) organization and angiogenesis. The GO terms for AFP linked it with the regulation of osteoblast and fat differentiation, as well as with brown fat cell differentiation and cold-induced thermogenesis, the latter also being a term shared with CLFP and GFP. Fat metabolism is crucial in the first hours postpartum, in preparation for starvation and thermoregulation.[1,42] Additionally, AFP GO terms related it to myeloid and B cell differentiation, branching morphogenesis – a key feature of vessel formation and glial cell differentiation. The GO terms for SFP are related to cell migration and adhesion, regulation of nitric oxide synthesis, leukocyte differentiation, coagulation and wound healing. GFP displays GO terms associated with ossification, osteoblast differentiation, response to mechanical stimulus, fibroblast proliferation, cartilage development, hormonal regulation and glucose homeostasis.[2] CLFP is also associated with bone mineralization, ossification, glial cell migration (along with SFP), regulation of muscle cell differentiation and axon guidance. This diverse range of potential functions supports a pivotal role for perinatal fibroblastic clusters in the bone under construction and the transition to postnatal life. In support for these broad organizing functions, we noted that the perinatal fibroblastic cluster signatures include genes previously identified in the blastema formed after digit tip amputation in adult mice. These genes include *Mest1*, *Ltbp2*, *Scara5*, *Clec3b* and *Cd34*, with the latter three being expressed in dermal-derived fibroblasts (Figure 3c and Supplementary figure 5).[11,12]

Interactions between endochondral cell subsets and implications for central tolerance

To gain insight into the interconnectivity of the different perinatal bone cell populations, we used CellPhoneDB, an algorithm based on the expression pattern of ligands, receptors and ECM components, therefore capturing both direct and indirect interactions.[43] The degree of interaction within mesenchymal clusters (MC-MC) and between mesenchymal clusters and endothelial cells (MC-EC) or hematopoietic clusters (MC-HC) is shown in Figure 4a. Across all three compartments, cluster interactions were more prominent at E18.5 than at PN1.

MC-MC interactions displayed the highest number of calls, with TC, OsC, SFP and GFP being the most interacting clusters, and Myo the least. ECM components such as collagens and integrins were the most abundant predicted connectors, as expected for fibroblastic populations, and exhibiting several stage-specific differences (Supplementary tables 2–4). The types of collagens and integrin complexes varied greatly, with different clusters exhibiting specific profiles (Supplementary table 4). This variation fits the dynamic properties of the matrisome, which changes according to age and inflammatory conditions.[44] For example, a significant difference between E18.5 and PN1 was the lack of expression of the integrin α1β1 complex at PN1 in the GFP, ACP and OsC clusters. This integrin complex is associated with remodeling and wound healing.[45] Membrane-bound Col13a1, which is important for bone growth, was predominantly expressed by the OsC and EC clusters.[46] This analysis also identified the interconnection of SC with several other subsets through Col20a1 and α1β1/α2β1 integrin complexes. *Col20a1* is specific to SC and expressed only at perinatal stages (Supplementary figures 1 and 2 and nicheview.shiny.embl.de). Given that the ECM participates in signaling, migration, lineage specification and compartmentalization in several tissues,[47] the changes we observed may dictate a code involved in the spatial and temporal organization of the skeletal program.

Next, we explored direct interactions (no secreted molecules; *P*-value < 0.05) and focused on those clusters that displayed the highest number of partners and the strongest connectors (Figure 4b; all direct connectors are provided in Supplementary tables 5 and 6). Within the MC, the SFP and OsC clusters emerged as the most dynamic, with Cadm1 and Col13a1 mediating significant interactions in the latter. NOTCH and their ligands were highly expressed among fibroblastic clusters, as expected from their important roles in bone development and homeostasis.[48] Dlk1-Notch1 and Dlk1-Notch2 mediated very strong connectors across all mesenchymal clusters and with EC (Supplementary tables 5 and 6). Dlk1 is a non-canonical ligand that inhibits Notch1 receptor activity.[49] Notably, *Dlk1* is not expressed in adult bone (nicheview.shiny.embl.de[15]), but is restricted and highly expressed in most mesenchymal clusters at perinatal stages. Notch3 mediated various putative connectors, mainly in AFP, which is relevant considering *NOTCH3* mutations cause Lateral Meningocele Syndrome (OMIM #130720), which is characterized by several skeletal abnormalities.[48] In addition, the highly prevalent pair could play a role in vasculature remodeling, as slow-cycling LepR:Cre *Notch3*+ cells are closely associated with vasculature in the bone marrow of adult mice.[35] In fact,
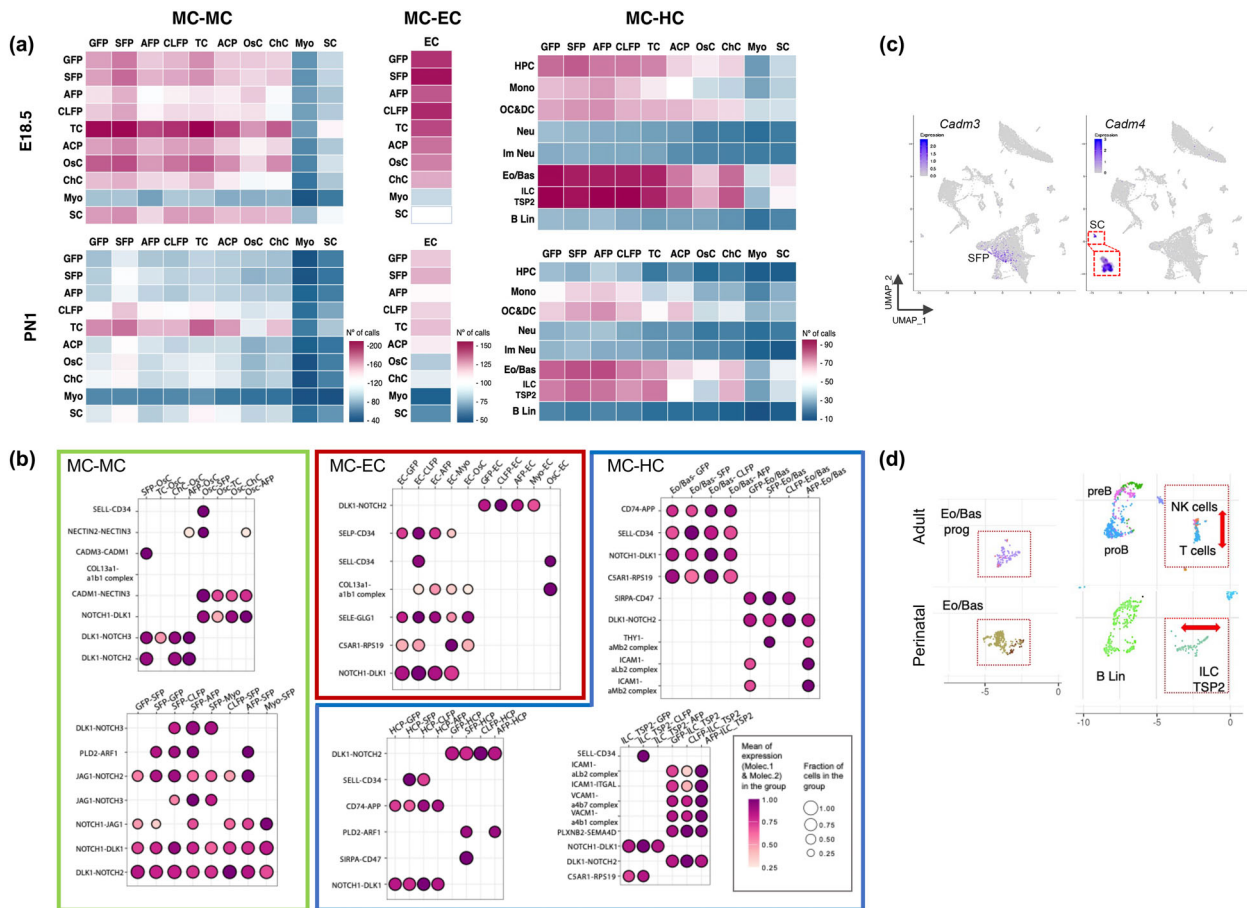
Figure 4. Cell to cell communication in the perinatal endochondral bone. **(a)** Heatmap showing the total number of connections (No. of calls; P-value ≤ 0.05) identified by the CellPhoneDB algorithm within mesenchymal clusters (MC-MC), between mesenchymal clusters and endothelial cells (MC-EC) and between mesenchymal and hematopoietic clusters (MC-HC). **(b)** Bubble plot representation of selected putative direct interactions (rows) inferred with CellPhoneDB (no secreted molecules; P-value ≤ 0.05) at E18.5 showing the mesenchymal clusters with the higher number of associations within the mesenchymal compartment (MC-MC), with endothelial cells (MC-EC) and with hematopoietic clusters (MC-HC). The size of each dot represents the mean fraction of cells in the group (cluster1 and cluster 2) expressing molecule 1 and molecule 2. Color encodes the scaled mean expression levels of interacting molecules in the group. **(c)** UMAP projection at E18.5 showing the exclusive expression of *Cadm3* and *Cadm4* in the SFP and SC clusters, respectively, a putative direct interaction identified by CellPhoneDB analysis. **(d)** UMAP coordinates comparing Eo/Bas, NK-Tcells *versus* ILC-TSP2 and B-cell clusters in perinatal and adult bone. Striking differences are observed between NK-T cells and ILC-TSP2 (enclosed in a red box and indicated by red arrows).

the EC connectome (also explored at E18.5[50]), displayed a high number of direct predicted interactions with GFP, OsC, AFP, CLFP and Myo, primarily through selectins (SELL, SELP, SELE). This supports our previous GO analyses that associated AFP and CLFP with different aspects of angiogenesis (Figure 4b and Supplementary figure 7). Schwann cells (SC) also showed broad potential for direct interactions with SFP, AFP, OsC, CLFP and with themselves (Supplementary table 5). In particular, we identified a specific link mediated by Cadm3 (exclusive to SFP) and Cadm4 (exclusive to SC; Figure 4c). Future studies will be needed to determine

the relevance of this interaction. Of note, *CADM3* mutations are associated with type 2FF Charcot–Marie–tooth disease (OMIM #619519), a peripheral neuropathy characterized by early childhood onset, progressive weakness and muscle atrophy.[51] In this context, both *Col20a1* and *Cadm4* are excellent candidate *loci* for the design of genetic tools to study how the peripheral nervous system regulates endochondral bone development and regeneration.[52]

In the hematopoietic compartment, several of the MC clusters were predicted to interact with HPC, and preferentially with Eo/Bas and ILC-TSP2, with GFP, SFP,

AFP and CLFP being the most active (Figure 4a). Representative direct connectors for HPC, ILC-TSP2 and Eo/Bas include App-CD74, Icam1-Itgal and Sell-CD34, respectively (Figure 4b and Supplementary table 6). While adult/perinatal Eo/Bas and B lineage cells map to equivalent coordinates in the UMAP space, significant differences exist between perinatal ILC-TSP2 cells and adult NK and T cells (Figure 4d and Supplementary figure 8). T cells in the adult BM correspond to memory T cells and regulatory T cells.[53] The T cell cluster in the adult scRNA-seq dataset (nicheview.shiny.embl.de[15]) expresses highly all CD3 components of the TCR receptor (*Cd3e, Cd3g, Cd3d* and *Cd247*/TCR zeta), along with *Cd8a* and *Cd8b1*, identifying them mostly as memory CD8 T cells. In contrast, perinatal ICL-TSP2 cells only transcribe *Cd3g* and *Cd247*, do not express *Lef1*[54] and lack expression of the central memory T cells markers *Sell*/CD62L and *Ccr7*.[55] In line with recent scRNAseq data on thymus seeding progenitors (TSP), we named this cluster ILC-TSP2, based on the expression of *Cd7, Itgb7, Irf8, CD3e (CD3g* in mice) and the absence of *Hoxa9* and *Cd34* transcripts.[56,57] Of note, we identified ILC-TSP2 as the only cluster expressing *Ccl5* (Supplementary figures 1 and Supplementary figure 8). This is relevant because callus formation in bone fracture models depends on the expression of the Ccl5 receptors Ccr5 and Ccr3 in periosteal Mx1$^+$*Acta2*/αSMA$^+$ cells,[58] which underscores the relevance of the crosstalk between the mesenchymal and hematopoietic compartments (see also additional ILC-TSP2 markers in Supplementary figure 1). The role of the Eo/Bas cluster at these stages is less characterized. Perinatal Eo/Bas cells specifically express high levels of the anti-inflammatory interleukins *Il4* and *Il13* (Supplementary figures 1 and 8). In keeping with an anti-inflammatory setup, we also observed the lack of expression of MHCII genes (*H2-Aa* and *H2-Eb1*) in monocyte and dendritic cells (Mon DC), and a high expression of *Il1rn* and *Il1r2* (both encoding decoy receptors of pro-inflammatory IL1) in monocytes and neutrophil clusters. In addition, monocyte, neutrophil and Eo/Bas clusters express high levels of *Osm* (Oncostatin M), known to stimulate osteogenesis and to inhibit adipogenesis,[8] further emphasizing the interdependence of the different cellular components (Supplementary figure 8).

Main transcriptional networks and immunomodulatory properties of the mesenchymal compartment within the perinatal endochondral bone

To elucidate the transcriptional programs operating in the mesenchymal compartment, particularly within the fibroblastic clusters, we utilized SCENIC (Single-Cell rEgulatory Network Inference and Clustering).[59] This tool is capable of detecting the activation of gene regulatory networks controlled by a given transcription factor [referred to as "regulons", denoted with a (+) symbol] based on the expression of its cognate target genes, even in those cases where the upstream transcription factor itself was not captured in the scRNA-seq data. Conversely, if not sufficient transcriptional targets are detected, SCENIC labels the regulon as inactive, regardless of whether the controlling transcriptional regulator is expressed. The top ten regulons at E18.5 and PN1, along with those differentially active between stages, are shown in Supplementary figure 9. SCENIC accurately captured biologically relevant regulons in chondrogenic [Sox9(+), Sox5(+); ChC and ACP], osteogenic [Runx2(+), Sp7(+), Dlx5(+); OsC] and adipogenic [Pparg(+), Gata6(+), Prdm6(+); AFP and GFP] clusters (Supplementary figure 10). Concerning the latter differentiation program, *Pparg* is a key adipogenic regulator, while *Gata6* has been recently associated with brown adipogenesis,[60] in agreement with our GO analysis. Finally, GWAS studies have linked *PRDM6* to obesity and osteoporosis,[61] while another family member, *Prdm16*, has been implicated in brown fat differentiation in early myoblast progenitors.[62] The CLFP population shared several active regulons with the Myo cluster [MyoG(+), Msc(+), Myf5(+) and MyoD(+)], suggesting a potential relationship between these two populations. Mkx(+) was identified as the most-significant regulon in the TC cluster (Figure 3).[63] Two additional key observations could be extracted from the SCENIC analysis. Firstly, several Hox regulons were active in GFP, SFP, TC and ACP clusters (Supplementary figure 9). While *Hox* functions have been mostly studied in the context of axial and limb patterning, it has been observed that periosteal Hox$^+$ fibroblastic populations contribute to bone repair in adult fracture models.[64] Secondly, several of the most prominent regulons active in the SFP and ACP clusters were related to inflammation and exhibited multiple cross-regulatory interactions (tables in Figure 5a, b). *Nfkb1*, one of the most prominent regulons identified by SCENIC, encodes p105 and its processed form, p50. Dimers of p65 (the class 2 subunit of the NF-κB transcription factor, encoded by *RelA*) and p50 are known to trigger a pro-inflammatory response. The NF-κB pathway is negatively controlled by p50/p50 homodimers that can outcompete p65/p50 dimers and also suppress pro-inflammatory gene expression through association with other proteins such as HDACs and p300.[65] These p50/50 homodimers can also promote the expression of anti-inflammatory genes by associating with Bcl3.[66] The Bcl3(+) regulon is itself active at E18.5 and PN1 and controls *Nfkb1* expression (Figure 5a, b and Supplementary figure 9). Another
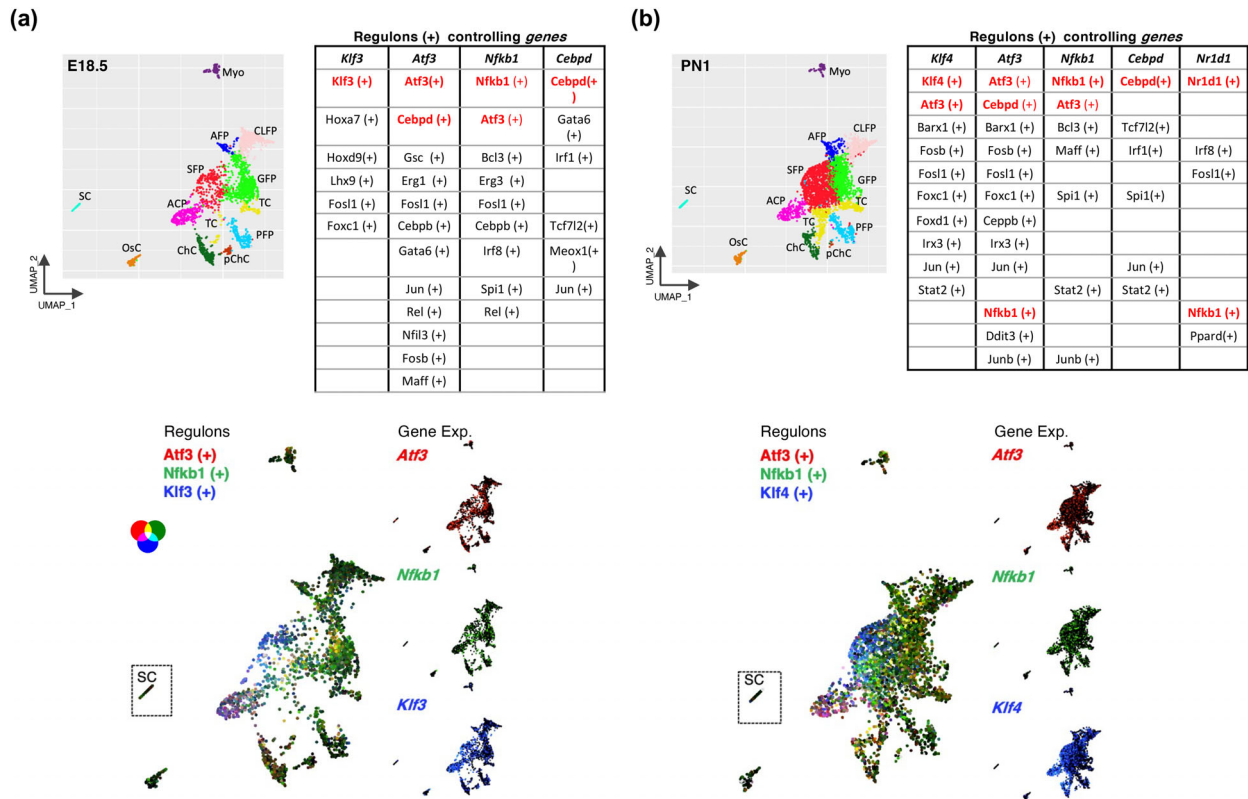
(a)

Regulons (+) controlling *genes*

Klf3	Atf3	Nfkb1	Cebpd
Klf3 (+)	**Atf3(+)**	**Nfkb1 (+)**	**Cebpd(+)**
Hoxa7 (+)	**Cebpd (+)**	Atf3 (+)	Gata6 (+)
Hoxd9(+)	Gsc (+)	Bcl3 (+)	Irf1 (+)
Lhx9 (+)	Erg1 (+)	Erg3 (+)	
Fosl1 (+)	Fosl1 (+)	Fosl1 (+)	
Foxc1 (+)	Cebpb (+)	Cebpb (+)	Tcf7l2(+)
	Gata6 (+)	Irf8 (+)	Meox1(+)
	Jun (+)	Spi1 (+)	Jun (+)
	Rel (+)	Rel (+)	
	Nfil3 (+)		
	Fosb (+)		
	Maff (+)		

(b)

Regulons (+) controlling *genes*

Klf4	Atf3	Nfkb1	Cebpd	Nr1d1
Klf4 (+)	**Atf3 (+)**	**Nfkb1 (+)**	**Cebpd(+)**	**Nr1d1 (+)**
Atf3 (+)	**Atf3 (+)**			
Barx1 (+)	Barx1 (+)	Bcl3 (+)	Tcf7l2(+)	
Fosb (+)	Fosb (+)	Maff (+)	Irf1(+)	Irf8 (+)
Fosl1 (+)	Fosl1 (+)			Fosl1(+)
Foxc1 (+)	Foxc1 (+)	Spi1 (+)	Spi1(+)	
Foxd1 (+)	Ceppb (+)			
Irx3 (+)	Irx3 (+)			
Jun (+)	Jun (+)		Jun (+)	
Stat2 (+)		Stat2 (+)	Stat2 (+)	
Nfkb1 (+)				**Nfkb1 (+)**
	Ddit3 (+)			Ppard(+)
	Junb (+)		Junb (+)	

Figure 5. Immunomodulatory properties of the perinatal bone mesenchymal compartment. **(a, b)** SCENIC analysis of the mesenchymal compartment at E18.5 **(a)** and PN1 **(b)**, displaying the main immunomodulatory regulons identified. UMAP projections of the mesenchymal clusters at E18.5 and PN1 are shown as a guide for cluster identification. The tables show the regulons that control the expression of key transcription factors involved in immunomodulation (*Klf3*, *Klf4*, *Nfkb1*, *Cebpd* and *Nr1d1*). Colored in red are their regulons to show their autoregulation and the network of cross-regulation. The lower panels depict the joint activity of the Atf3(+), Nfkb1(+) and Klf3(+) regulons at E18.5 and of the Atf3(+), Nfkb1(+) and Klf4(+) regulons at PN1. The individual expression of the corresponding genes is displayed to the right of each SCENIC projection.

active regulon involved in the regulation of inflammation, Atf3(+),[67] is also active at both E18.5 and PN1. Atf3 is known to inhibit the NF-κB pathway by forming dimers with p65 and recruiting HDAC1.[68] *Klf3* is a transcriptional repressor that directly suppresses *RelA* expression,[69] and its regulon is active exclusively at E18.5. Notably, the Klf4(+) regulon is detected as active at PN1. Beyond its role in osteogenesis,[70] Klf4 is involved in various cellular processes depending on the cell type and context, and can function as either a pro- or anti-inflammatory factor.[71,72] The Cebpd(+) regulon modulates various cellular processes and is mainly associated with the inflammatory response in macrophages, but it can also act in preventing deleterious effects of the inflammatory response.[73] Another regulon that is active exclusively at PN1 and linked to inflammatory regulation is Nr1d1(+). *Nr1d1*/*Rev-Erbα* encodes a core protein of the circadian clock.[74,75] Interestingly, and still underexplored, different *Hox* genes

interact with the NF-κB pathway and play roles in different aspects of inflammation.[76]

Strategies for the prospective isolation of mesenchymal populations

Based on their molecular profiles, the well-characterized PαS population [immunophenotype: Lineage negative (CD45, TER119, CD31) and PDGFR-α$^+$, Sca-1$^+$] corresponds to the SFP, ACP, and part of the GFP clusters. PαS were first described in adult bone[77] and these Sca-1$^+$ (encoded by *Ly6a*) fibroblastic populations have been shown to contain multipotent progenitors able to give rise to cartilage, bone and adipose tissue.[77–79] In addition, Sca1$^+$ cells in the periosteum have been shown to highly contribute to callus formation in bone fracture models.[6,35,40,80] PαS are most abundant at perinatal stages, peaking immediately after birth and becoming less represented in adult mice.[78] These properties, together
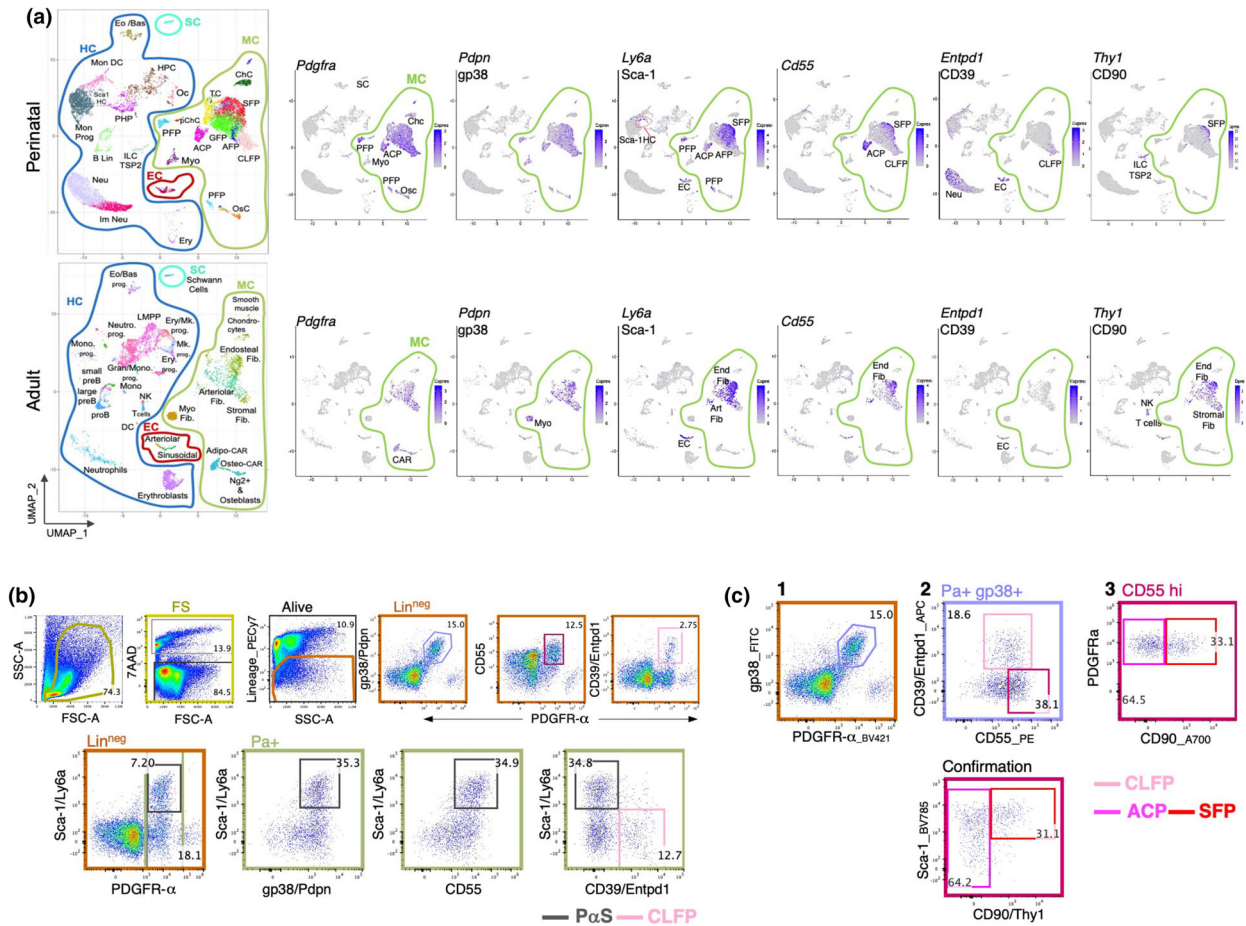
Figure 6. Prospective identification of ACP, SFP and CLFP clusters in newborns. **(a)** Expression of surface markers suitable for FC analysis at perinatal stages. PaS (PDGFRa$^+$, Sca-1$^+$) cells encompass the SFP and ACP clusters. In addition, *Ly6a*/Sca1 is expressed in EC and Sca1-HC. *Cd55* mirrors well the expression of *Ly6a* in the mesenchymal clusters. Within mesenchymal clusters, *Entpd*/Cd39 mainly identifies CLFP, while *Thy1*/CD90 is restricted to SFP. The expression of these genes in adult bone is shown in the bottom row. **(b)** FC analysis comparing the expression of Sca-1 with that of other prospective markers (CD55, CD39 and CD90) in the mesenchymal compartment (Lin^{neg} PDGFR-a$^+$/Pa$^+$ and gp38/Pdpn$^+$). Dead cells were excluded as 7-AAD positive. Lin = Lineage (TER119, CD45 and CD31). **(c)** A three-step strategy that does not rely on the use of Sca-1 to enrich in SFP, ACP and CLFP populations. SFP (Lin^{neg} PDGFRa$^+$ gp38$^+$ CD39^{neg} CD55$^+$ CD90$^+$); ACP (Lin^{neg} PDGFRa$^+$ gp38$^+$ CD39^{neg} CD55$^+$ CD90^{neg}); CLFP (Lin^{neg} PDGFRa$^+$ gp38$^+$ CD39^{pos}). The pseudocolor plots shown are representative of at least three independent experiments at PN1, with each cell sample extracted from 3 or 4 littermates. Similar results were obtained with E18.5 samples (data not shown).

with the immunomodulatory profile of SFP and ACP as revealed by the SCENIC analysis, position PaS as an important target for biomedical applications. Therefore, developing robust isolation strategies for the human equivalent populations will be crucial for their use in cellular therapies. However, since there is no human ortholog of the *Ly6a*/Sca-1 gene,[81] additional reliable markers need to be identified. To do so, we interrogated our scRNA-seq datasets for several surface markers that were evolutionary conserved between mice and humans and validated them by flow cytometry (FC) to develop an alternative isolation strategy that enriches in PaS cells without relying on the use of Sca-1 antibodies. The final

strategy and optimal markers used to enrich in SFP, ACP and CLFP populations from newborn bone are shown in Figure 6. All lineage negative *Ly6a*/Sca-1$^+$ cells were PDGFR-a$^+$ (Pa$^+$), *Pdpn*/gp38$^+$, CD55$^+$ and mostly *Entpd1*/CD39 negative (Figure 6a). CD39$^+$ Pa$^+$ defined the CLFP population, while CD55 was highly expressed in both ACP and SFP, with *Thy1*/CD90 exclusively labeling SFP (Figure 6a, b). These profiles allowed the development of a strategy to purify CLFP, SFP and ACP populations in three steps (Figure 6c). The separation between SFP (CD90$^+$) and ACP (CD90^{neg}) within CD55^{hi} cells was confirmed using Sca-1 and CD90 staining. While this strategy is suitable for perinatal stages,

Entpd1/CD39 is minimally expressed in mesenchymal adult populations (Figure 6a), which illustrates the necessity of performing ontogenic studies and tailoring the prospective immunophenotype to the specific developmental stage being analyzed.

DISCUSSION

As previous scRNAseq studies have shown, the adult bone mesenchymal compartment is highly diverse, and this resource study uncovers how such complexity starts to build up in early life. Our analysis identifies different clusters of fibroblastic populations at perinatal stages, each with diverse potentials as indicated by GO and gene regulatory network tools. These analyses revealed that the most closely related fibroblastic clusters (GFP, SFP, AFP and CLFP), besides their potential roles in regulating osteogenesis, adipogenesis and chondrogenesis, may also be involved in a broad range of tissue-organizing functions, including the regulation of hematopoiesis, angiogenesis, innervation, extracellular matrix organization, metabolism and hemostasis. For instance, the representation of AFP increases after birth and, along with the GFP population, is associated with adipogenesis, including brown fat differentiation and cold-induced thermogenesis, which are crucial for managing caloric restriction and temperature regulation once the protection of the placenta is lost.[1] *Lepr*-expressing CAR cells, highly represented in adults, were not present at perinatal stages. This absence is not attributable to the enrichment strategy used, since this population was barely detected by FC from total bone enzymatic cell suspensions by using the Adipo-CARs marker CD106/Vcam1 (data not shown). Our findings are in line with other studies,[38,50] which show that Adipo-CARs are absent at E18.5 and just emerging at postnatal day 4. Interestingly, AFP might contain Adipo-CAR precursors, since it was the main and almost exclusive cluster expressing *Notch3*. *Notch3*-expressing cells labeled by LepR: Cre in adults have been shown to be multipotential, slow-cycling cells.[35] Two other clusters that became more prominent after birth were the SFP and TC populations. While the absence of an equivalent TC cluster in adults could be due to differences in sample preparation methods or bone origin, both TC and several fibroblastic clusters exhibited differential molecular fingerprints previously identified as specific of the blastema during digit tip regeneration in adult mice (e.g. *Mest* expression). These results fit the previous observation that digit tip blastema cells are more similar to PN3 bone-derived mesenchymal cells than to those of adults and significantly differ from those in the limb bud.[12] In amphibian limb amputation models, successful regeneration requires the dedifferentiation of connective tissue and dermal fibroblasts

in order to rebuild the skeleton.[13] Hence, the complex array of perinatal fibroblastic populations we have identified in this study, some exhibiting dermal signatures, may act as organizers of reprogramming, specification and differentiation of bone structure during these dynamic stages in which osteo-chondrogenic programs are highly active and the bone marrow is under active construction to establish definitive hematopoiesis. The granularity of our study allowed the identification of various fibroblastic populations, each with distinct molecular identities and putative roles in organizing these processes. Our profiling of markers and active gene regulatory networks provides a starting point for the prospective isolation – as we show for SFP, ACP and CLFP – and *in vitro* expansion of specific cell subsets for tissue engineering applications. Besides, the identification of cluster-specific genes will enable the design of more precise inducible genetic mouse models for cell fate tracking or cell population depletion. As the system reaches the steady state after sexual maturity, these fibroblastic populations become less abundant in the inner BM, and become restricted to the endosteum and periosteum, being mainly extracted by enzymatic digestion of bone chips.[80] Concurrently, BMSC, such as *Lepr*-expressing CARs, become more prominent.[6,7,35,37] Only when the steady state balance is disrupted, as observed after bone fracture, do periosteal cells (e.g. those with the PαS immunophenotype) and possibly nearby connective tissue cells[13] reactivate the endochondral bone program for callus formation.[6,9,40,80]

Our integral approach to capture all endochondral bone cell populations allowed us to predict both intra- and inter-compartment interactions among all mesenchymal clusters. For instance, in this study, we identified that *Cadm3*, the ortholog of the human gene mutated in Charcot–Marie-tooth type 2FF peripheral neuropathy,[51] is specifically expressed by the SFP population and mediates a putative direct interaction with Schwann cells *via* Cadm4. These analyses also unveiled a potentially complex MC-HC connectome, inferring interactions of fibroblastic SFP, AFP, CLFP and GFP populations with HPC and, more unexpectedly, with the ILC-TSP2 and Eo/Bas clusters. From the immune perspective, these ILC-TSP2 interactions might play a role in the protection/maturation of TSP for the onset of the central tolerance and the generation of the first thymic regulatory T cells.[82,83] This hypothesis is supported by the recent identification of two mesenchymal cell populations essential for thymus development and exhibiting prospective signatures similar to those of the bone-derived GFP and SFP clusters.[84] Regarding the Eo/Bas cluster, we observed a high and exclusive expression of anti-inflammatory cytokines *Il4* and *Il13*. In line with our findings, other studies have shown that basophil cells in

newborns skew the differentiation of T cells towards Th2, which in newborns have an anti-inflammatory profile to protect intestinal microbiota and to prevent tissue damage.[85] Highlighting the predicted interdependence between compartments, both of these hematopoietic clusters express key factors involved in bone healing (*Ccl5*[58] in ILC-TSP2) and in balancing osteogenesis and adipogenesis (*Osm*[8] in Eo/Bas). Future studies will be required to explore the potential significance of these bidirectional interactions during perinatal, puberty and adult stages.

Another important finding from our study is the identification of several immunomodulatory transcriptional programs operating in mesenchymal clusters (SFP, ACP, and, to a lesser extent, GFP) that seem to be skewed towards an anti-inflammatory response. These observations fit the earlier proposal that the 2 week juvenile mouse bone provides an anti-inflammatory environment, characterized by low expression of MHCI molecules in stromal populations, which shifts to a pro-inflammatory state after sexual maturation.[44] In support of this idea, we found that several mesenchymal clusters highly express *Dlk1*, a ligand previously shown to inhibit Notch-dependent pro-inflammatory cytokine production in macrophages.[49] In contrast to adult populations, perinatal macrophages do not express MHCII genes (*H2E-b1* and *H2A-a*) nor their protein products (as confirmed by FC; data not shown), while perinatal neutrophils display high levels of expression of the Il-1 decoy receptors *Il1rn* and *Il1r2*. An attractive hypothesis stemming from our results is that an anti-inflammatory environment of the perinatal BM could ensure the proper balance between myeloid and lymphoid HSC lineage choice. High pro-inflammatory conditions promote HSC proliferation and skew their differentiation towards the myeloid lineage at the expense of lymphopoiesis, potentially leading to excessive proliferation and eventual exhaustion of HSC.[86] In addition, and particularly in early life, when individuals are first exposed to pathogens, primary immune organs (bone marrow and thymus) should be protected from infections and the harmful effects of a highly pro-inflammatory milieu to ensure the establishment of a proper self-tolerance.

Finally, our study reveals significant cellular and gene expression differences between neonatal and adult stages, which implies that therapeutic interventions targeting endochondral bone populations or compartments must be adapted according to the patient's age. While our work is limited by the lack of functional validation of the main findings and the fine spatial localization of each identified cluster, it provides a valuable resource that highlights key aspects of endochondral bone development, which need further in-depth analysis by the broader research community.

METHODS

Mice (*Mus musculus*)

Adult C57Bl/6J females and males were purchased from Envigo (Indianapolis, IN, USA) and housed under pathogen-free conditions according to Spanish and EU regulations. All animal experiments were designed and conducted according to the 3R principles and approved by the Universidad Pablo de Olavide Ethics Committee and the local authorities (license number 01-08-2018-123; Junta de Andalucía). Animals were set in natural matings, and vaginal plugs were checked to time the collection of samples at E18.5 and postnatal day 1, defining the day of birth as postnatal day 0. Individuals of both sexes were used for scRNA-seq experiments and flow cytometry studies.

Tissue processing for flow cytometry (FC)

Forelimb long bones (humerus, radius and ulna) were dissected from fetuses at embryonic day E18.5 and pups at postnatal day 1 and carefully cleaned of surrounding tissue. Cell suspensions for flow cytometry analysis or sorting were prepared as reported previously,[87] with the following specific modifications. For perinatal stages, bones were cut in small pieces with a scalpel and all tissue was processed (bone marrow cells were not washed out or flushed) for enzymatic digestion using collagenase D (2 mg mL^{-1} in DMEM [high glucose]). Red cell lysis was not performed. The digestion time for perinatal stages was 45–50 min in a water bath at 37°C with three rounds of gentle pipetting every 10 min to help disaggregation. Collagenase digestion was stopped by placing the tube on ice and by addition of ice-cold 10% FBS/HBSS+ (HBSS, 10 mM HEPES, 1% Penicillin–Streptomycin). Cells in suspension were recovered to a new tube and any remaining bone fragments were transferred to a ceramic mortar and 2 to 3 cycles of very gentle tapping with the pestle (20–30 times) were applied to maximize cell recovery. Cells from the mortar were recovered with 10% FBS/HBSS+, filtered through a 100 μm strainer, and pooled with the earlier cell suspension. Following centrifugation (350 *g* for 10 min at 4°C), the cells were resuspended in 2% FBS/HBSS+ for FC analysis or sorting. Before antibody staining, blocking of FcγR II/III was performed by incubating cells with anti-CD16/CD32 antibodies (1 μg per million cells) for 15 min on ice. Sorting collection tubes were pre-coated with 10% FBS/HBSS+ for 15 min on ice, and kept at 4°C during sorting.

Samples were analyzed and sorted using a SONY MA900 cell sorter (lasers: 488/561 and 405/638 nm). 7-AAD (7-amino actinomycin D) was the only dye used to discriminate dead cells. The lineage cocktail used to analyze mesenchymal populations included CD45 (hematopoietic cells), TER119 (erythroid cells) and CD31 (endothelial cells), all conjugated to biotin and detected *via* secondary staining with

Table 1. Antibodies used in this study

Antibody	Biolegend Cat. No.
FITC anti-mouse CD9 (clone MZ3)	124807
Brilliant Violet 421™ anti-mouse CD140a (clone APA5)	135923
APC anti-mouse CD140a (clone APA5)	135907
APC anti-mouse CD31 (clone 390)	102409
Brilliant Violet 785™ anti-mouse Ly-6A/E (Sca-1) (clone D7)	108139
Alexa Fluor 700 anti-mouse CD90.2 (Thy-1.2) (clone 53–2.1)	140323
FITC anti-mouse Podoplanin (clone 8.1.1)	127415
APC anti-mouse CD39 (clone Duha59)	143809
PE anti-mouse CD55 (DAF) (clone RIKO-3)	131803
Biotin anti-mouse TER-119/Erythroid Cells (clone TER-119)	116204
Biotin anti-mouse CD31 (clone 390)	102404
Biotin anti-mouse CD45 (clone 30-F11)	103104

Streptavidin-PECy7. Lowly expressed molecules were stained with antibodies conjugated either with BV421 (not used when PB was selected), PE or APC, while highly expressed molecules were stained with antibodies conjugated either with PB (not used when BV421 was selected), FITC, BV785 or A700 fluorophores. All antibodies (Biolegend, San Diego, CA, USA) used are listed in Table 1.

Flow cytometry analysis

Data were acquired with a SONY MA900 (Sony Biotechnology, San Jose, CA, USA) using the equipment's software and further analyzed with FlowJo version 10.8.0. Representative plots of at least three independent experiments are shown.

Generation of single-cell RNA-seq datasets

Five E18.5 fetuses and four PN1 newborns, all littermates, were processed for cell suspension preparation as described above. No sex discrimination was done, as gender-associated differences are not significantly relevant at perinatal stages. After eliminating dead cells and multiplets by electronical gating, the different fractions of sorted cells (100 µm nozzle) were mixed in the proportions detailed in Figure 1a. Cells were sorted in excess (approximately 5 times the calculated amount) to compensate for potential cell loss. The absence of cell aggregates was verified by microscopic visualization, and cell number and viability were assessed using a TC-20 cell counter (Bio-Rad) after trypan blue staining. For both E18.5 and PN1 samples, viability was over 90%. The cells were resuspended in HBSS+ 2% FBS at 800 cells µL^{-1} and 20.000 cells were loaded onto a Chromium Controller G chip (10× Genomics, Pleasanton, CA, USA) and processed using the Chromium Next GEM Single Cell 3′ Kit v3.1 for the generation of the scRNAseq libraries, according to the manufacturer's instructions. Sequencing (PE100/100/10/10) was performed on a DNBSEQ-T7 system (BGI Group, Shenzhen, China). Sequencing depth was 43 005 and 43 398 reads/cell at E18.5 and PN1, respectively (60% saturation). It should be noted that this kit captures the 3′UTR of transcripts, and therefore cannot detect alternative transcript isoforms.

Analysis of single-cell RNA-seq datasets

Pre-processing of scRNAseq data

Reads were aligned to the mouse genome (mm10) using Cell Ranger v6.0 software. Cells with fewer than 400 or more than 6000 detected genes, as well as those with more than 10% mitochondrial reads, were excluded. For normalization, log-transformation with a scale factor of 10 000 was applied.

Dimensional reduction and clustering

The top 2000 high variable genes (HVG) were identified using the "vst" method in the *FindVariableFeatures* function of the Seurat package (version 4.0.3[88]). Following data scaling, PCA (Principal Component Analysis) with 30 principal components (PCs) was performed. Cells were clustered using the Louvain method on a nearest neighbor graph using the *FindClusters* and *FindNeighbors* in Seurat. A UMAP on the PCA-reduced data was performed to visualize the clusters.

Elimination of erythroid cells and doublets

Erythroid cells were identified and removed from downstream analyses based on specific gene markers. For doublet removal, DoubletFinder software[89] was used. After filtering low-quality cells, putative doublets and erythroid cells, our dataset contained 7272 cells with a mean of 10 656 UMIs and 2625 genes for the E18.5 time point, and 7277 cells with a mean of 9827 UMIs and 2533 genes for the PN1 library. As both datasets were generated by pooling littermates of both sexes, we used the expression of sex-specific genes (*Xist, Esr1* and *Esr2* [female]; *Ddx3y, Eif2s3y, Kdm5d* and *Uty* [male][90]) to identify whether any given cell was derived from a female or a male individual. A cell was assigned as "female" or "male" if it had at least one read from a female or male specific transcript, respectively. Cells with at least one read from both male and female specific transcripts were tagged as "undetermined". Cells without any sex-specific transcript reads were labeled as "NA". In the E18.5 sample, we identified 21% female cells, 42% male cells, 3.7% undetermined and 33.3% NA cells. In the PN1 sample, 42.3% female cells, 28.1% male cells, 4.4% undetermined and 25.2% NA cells were identified.

Sample integration

For the joint analysis of the E18.5 and PN1 samples, data were integrated using Harmony software[29] and projected into a

shared 2D UMAP embedding. Briefly, the Harmony algorithm integrates samples by accounting for multiple experimental and biological factors using an iterative four-step approach: (1) PCA for a low-dimensional embedding of cells from the different samples, followed by soft clustering to assign cells to potentially multiple clusters, favoring clusters with cells from multiple samples; (2) Global and sample-specific centroids are calculated for each cluster; (3) Centroids are used to compute linear correction factors; and (4) Finally, Harmony corrects each cell with a cell-specific factor that is a linear combination of sample correction factors weighted by the soft cluster assignment of the cell. For the comparison of perinatal and adult bone, we used Harmony to integrate both perinatal samples with the adult dataset.[15] The adult data set is available for download as a Seurat object from https://nicheview.shiny.embl.de.

Cell type annotation

Marker genes described in the extensive literature were used for cluster identification. While most of the cell types were annotated using a given clustering resolution, further refinement was achieved through sub-clustering (*FindSubCluster* function of Seurat) and re-annotation.

Inference of cell–cell interactions

CellPhoneDB v.2[43] was used to infer cell–cell connections. To prepare the data for CellPhoneDB analysis, mouse gene IDs were converted to their human orthologs, and count data were exported in h5ad format. The statistical analysis within CellPhoneDB evaluated significant interactions between predefined cell type pairs. For quantifying the total number of interactions, a P-value threshold of ≤ 0.05 was selected. For direct interactions (Supplementary tables 5 and 6), we considered only connectors with no secreted molecules and P-value ≤ 0.05 and Log_2 mean > -1.

Gene regulatory network analysis

Mesenchymal clusters were extracted and reprocessed as described previously (i.e. HVG, PCA, clustering, UMAP). Inference of gene regulatory networks and regulon analysis was performed using pySCENIC software v.0.11.2[59] with default settings.

Gene ontology analysis

Differentially expressed genes (DEG) for each of the mesenchymal GFP, SFP, AFP and CLFP clusters at E18.5 and PN1 were identified using the FindAllMarkers() function in Seurat, with default parameters (by default Seurat uses the Wilcoxon Rank Sum test for statistical testing). The test was run separately for each timepoint, and the resulting DEG were filtered to include only genes with an adjusted P-value < 0.005. The resulting counts of genes used for GO analysis at E18.5/PN1 (Supplementary table 1) were 218/280 (AFP), 455/480 (CLFP), 185/234 (GFP) and 436/305

(SFP). The GO terms for the "Biological Process" category were retrieved from http://geneontology.org, filtered using a ratio Fold Enriched/Expected ≥ 2 and manually curated. Plots were generated using the ggplot2 tool for R, representing the $-\log_{10}$ (P-values < 0.05), and the overlap was calculated based on the number of genes identified in the GO term for each cluster.

AUTHOR CONTRIBUTIONS

Alejandro Díaz Rueda: Formal analysis; investigation; writing – review and editing. **Irepan Salvador-Martínez:** Formal analysis; software; writing – review and editing. **Ismael Sospedra-Arrufat:** Investigation; writing – review and editing. **Ana Alcaina-Caro:** Investigation; writing – review and editing. **Ana Fernández-Miñán:** Investigation; writing – review and editing. **Ana M Burgos-Ruiz:** Investigation; writing – review and editing. **Ildefonso Cases:** Investigation; writing – review and editing. **Alberto Mohedano:** Investigation; writing – review and editing. **Juan J Tena:** Formal analysis; funding acquisition; supervision; writing – review and editing. **Holger Heyn:** Funding acquisition; supervision; writing – review and editing. **Javier Lopez-Rios:** Conceptualization; funding acquisition; investigation; project administration; supervision; writing – original draft; writing – review and editing. **Gretel Nusspaumer:** Conceptualization; formal analysis; funding acquisition; investigation; project administration; supervision; writing – original draft; writing – review and editing.

CONFLICT OF INTEREST

The authors declare no conflicts of interest.

DATA AND CODE AVAILABILITY STATEMENT

Single-cell RNA-seq data have been deposited in the GEO database (accession number GSE232202) and are publicly available as of the date of publication. Flow cytometry data reported in this paper will be shared by the corresponding authors upon request.

All scripts necessary to replicate our analysis are available in the following Github repository (https://github.com/irepansalvador/stromal_cells.git), and are publicly available as of the date of publication.

REFERENCES

1. Hillman NH, Kallapur SG, Jobe AH. Physiology of transition from intrauterine to extrauterine life. *Clin Perinatol* 2012; **39**: 769–783.

2. Morton SU, Brodsky D. Fetal physiology and the transition to extrauterine life. *Clin Perinatol* 2016; **43**: 395–407.

3. Bianco P, Robey PG. Skeletal stem cells. *Development* 2015; **142**: 1023–1027.

4. Long F, Ornitz DM. Development of the endochondral skeleton. *Cold Spring Harb Perspect Biol* 2013; **5**: a008334.

5. Galea GL, Zein MR, Allen S, Francis-West P. Making and shaping endochondral and intramembranous bones. *Dev Dyn* 2021; **250**: 414–449.

6. Jeffery EC, Mann TLA, Pool JA, Zhao Z, Morrison SJ. Bone marrow and periosteal skeletal stem/progenitor cells make distinct contributions to bone maintenance and repair. *Cell Stem Cell* 2022; **29**: 1547–1561.

7. Shu HS, Liu YL, Tang XT, *et al.* Tracing the skeletal progenitor transition during postnatal bone formation. *Cell Stem Cell* 2021; **28**: 2122–2136.

8. Li Q, Xu R, Lei K, Yuan Q. Insights into skeletal stem cells. *Bone Res* 2022; **10**: 61.

9. Zhou X, von der Mark K, Henry S, Norton W, Adams H, de Crombrugghe B. Chondrocytes transdifferentiate into osteoblasts in endochondral bone during development, postnatal growth and fracture healing in mice. *PLoS Genet* 2014; **10**: e1004820.

10. Yang L, Tsang KY, Tang HC, Chan D, Cheah KS. Hypertrophic chondrocytes can become osteoblasts and osteocytes in endochondral bone formation. *Proc Natl Acad Sci USA* 2014; **111**: 12097–12102.

11. Johnson GL, Masias EJ, Lehoczky JA. Cellular heterogeneity and lineage restriction during mouse digit tip regeneration at single-cell resolution. *Dev Cell* 2020; **52**: 525–540.

12. Storer MA, Mahmud N, Karamboulas K, *et al.* Acquisition of a unique mesenchymal precursor-like blastema state underlies successful adult mammalian digit tip regeneration. *Dev Cell* 2020; **52**: 509–524.

13. Lin TY, Gerber T, Taniguchi-Sugiura Y, *et al.* Fibroblast dedifferentiation as a determinant of successful regeneration. *Dev Cell* 2021; **56**: 1541–1551.

14. Newton PT, Li L, Zhou B, *et al.* A radical switch in clonality reveals a stem cell niche in the epiphyseal growth plate. *Nature* 2019; **567**: 234–238.

15. Baccin C, Al-Sabah J, Velten L, *et al.* Combined single-cell and spatial transcriptomics reveal the molecular, cellular and spatial bone marrow niche organization. *Nat Cell Biol* 2020; **22**: 38–48.

16. Buenrostro JD, Corces MR, Lareau CA, *et al.* Integrated single-cell analysis maps the continuous regulatory landscape of human hematopoietic differentiation. *Cell* 2018; **173**: 1535–1548.

17. Ranzoni AM, Tangherloni A, Berest I, *et al.* Integrative single-cell RNA-Seq and ATAC-Seq analysis of human developmental hematopoiesis. *Cell Stem Cell* 2021; **28**: 472–487.

18. Akiyama H, Lefebvre V. Unraveling the transcriptional regulatory machinery in chondrogenesis. *J Bone Miner Metab* 2011; **29**: 390–395.

19. Komori T. Whole aspect of Runx2 functions in skeletal development. *Int J Mol Sci* 2022; **23**: e5776.

20. Alonso-Martin S, Rochat A, Mademtzoglou D, *et al.* Gene expression profiling of muscle stem cells identifies novel regulators of postnatal myogenesis. *Front Cell Dev Biol* 2016; **4**: 58.

21. Murchison ND, Price BA, Conner DA, *et al.* Regulation of tendon differentiation by scleraxis distinguishes force-transmitting tendons from muscle-anchoring tendons. *Development* 2007; **134**: 2697–2708.

22. Shukunami C, Takimoto A, Nishizaki Y, *et al.* Scleraxis is a transcriptional activator that regulates the expression of Tenomodulin, a marker of mature tenocytes and ligamentocytes. *Sci Rep* 2018; **8**: 3155.

23. Rees SG, Waggett AD, Kerr BC, *et al.* Immunolocalisation and expression of keratocan in tendon. *Osteoarthr Cartil* 2009; **17**: 276–279.

24. Pacifici M, Koyama E, Iwamoto M, Gentili C. Development of articular cartilage: what do we know about it and how may it occur? *Connect Tissue Res* 2000; **41**: 175–184.

25. Chijimatsu R, Saito T. Mechanisms of synovial joint and articular cartilage development. *Cell Mol Life Sci* 2019; **76**: 3939–3952.

26. Eschenbrenner E, Jouannet S, Clay D, *et al.* TspanC8 tetraspanins differentially regulate ADAM10 endocytosis and half-life. *Life Sci Alliance* 2020; **3**: e201900444.

27. Lima ILA, Silva JMD, Rodrigues LFD, *et al.* Contribution of atypical chemokine receptor 2/ackr2 in bone remodeling. *Bone* 2017; **101**: 113–122.

28. Decker RS, Um HB, Dyment NA, *et al.* Cell origin, volume and arrangement are drivers of articular cartilage formation, morphogenesis and response to injury in mouse limbs. *Dev Biol* 2017; **426**: 56–68.

29. Korsunsky I, Millard N, Fan J, *et al.* Fast, sensitive and accurate integration of single-cell data with harmony. *Nat Methods* 2019; **16**: 1289–1296.

30. Sugiyama T, Kohara H, Noda M, Nagasawa T. Maintenance of the hematopoietic stem cell pool by CXCL12-CXCR4 chemokine signaling in bone marrow stromal cell niches. *Immunity* 2006; **25**: 977–988.

31. Morrison SJ, Scadden DT. The bone marrow niche for haematopoietic stem cells. *Nature* 2014; **505**: 327–334.

32. Wolock SL, Krishnan I, Tenen DE, *et al.* Mapping distinct bone marrow niche populations and their differentiation paths. *Cell Rep* 2019; **28**: 302–311.

33. Tikhonova AN, Dolgalev I, Hu H, *et al.* The bone marrow microenvironment at single-cell resolution. *Nature* 2019; **569**: 222–228.

34. Matsushita Y, Nagata M, Kozloff KM, *et al.* A Wnt-mediated transformation of the bone marrow stromal cell identity orchestrates skeletal regeneration. *Nat Commun* 2020; **11**: 332.

35. Mo C, Guo J, Qin J, *et al.* Single-cell transcriptomics of LepR-positive skeletal cells reveals heterogeneous stress-dependent stem and progenitor pools. *EMBO J* 2022; **41**: e108415.

36. Severe N, Karabacak NM, Gustafsson K, *et al.* Stress-induced changes in bone marrow stromal cell populations revealed through single-cell protein expression mapping. *Cell Stem Cell* 2019; **25**: 570–583.

37. Mizoguchi T, Pinho S, Ahmed J, *et al.* Osterix marks distinct waves of primitive and definitive stromal progenitors during bone marrow development. *Dev Cell* 2014; **29**: 340–349.

38. Kara N, Xue Y, Zhao Z, *et al.* Endothelial and leptin receptor^{+} cells promote the maintenance of stem cells and hematopoiesis in early postnatal murine bone marrow. *Dev Cell* 2023; **58**: 348–360.

39. Baryawno N, Przybylski D, Kowalczyk MS, *et al.* A cellular taxonomy of the bone marrow stroma in homeostasis and leukemia. *Cell* 2019; **177**: 1915–1932.

40. Matthews BG, Novak S, Sbrana FV, *et al.* Heterogeneity of murine periosteum progenitors involved in fracture healing. *Elife* 2021; **10**: e58534.

41. Chan CK, Seo EY, Chen JY, *et al.* Identification and specification of the mouse skeletal stem cell. *Cell* 2015; **160**: 285–298.

42. Li Z, Bowers E, Zhu J, *et al.* Lipolysis of bone marrow adipocytes is required to fuel bone and the marrow niche during energy deficits. *Elife* 2022; **11**: e78496.

43. Efremova M, Vento-Tormo M, Teichmann SA, Vento-Tormo R. CellPhoneDB: inferring cell-cell communication from combined expression of multi-subunit ligand - receptor complexes. *Nat Protoc* 2020; **15**: 1484–1506.

44. Helbling PM, Pineiro-Yanez E, Gerosa R, *et al.* Global transcriptomic profiling of the bone marrow stromal microenvironment during postnatal development, aging, and inflammation. *Cell Rep* 2019; **29**: 3313–3330.

45. Carver W, Molano I, Reaves TA, Borg TK, Terracio L. Role of the α1β1 integrin complex in collagen gel contraction *in vitro* by fibroblasts. *J Cell Physiol* 1995; **165**: 425–437.

46. Ylonen R, Kyronlahti T, Sund M, *et al.* Type XIII collagen strongly affects bone formation in transgenic mice. *J Bone Miner Res* 2005; **20**: 1381–1393.

47. Long KR, Huttner WB. How the extracellular matrix shapes neural development. *Open Biol* 2019; **9**: 180216.

48. Zieba JT, Chen YT, Lee BH, Bae Y. Notch signaling in skeletal development, homeostasis and pathogenesis. *Biomolecules* 2020; **10**: e332.

49. Gonzalez MJ, Ruiz-Garcia A, Monsalve EM, *et al.* DLK1 is a novel inflammatory inhibitor which interferes with NOTCH1 signaling in TLR-activated murine macrophages. *Eur J Immunol* 2015; **45**: 2615–2627.

50. Liu Y, Chen Q, Jeong HW, *et al.* A specialized bone marrow microenvironment for fetal haematopoiesis. *Nat Commun* 2022; **13**: 1327.

51. Rebelo AP, Cortese A, Abraham A, *et al.* A CADM3 variant causes Charcot-Marie-Tooth disease with marked upper limb involvement. *Brain* 2021; **144**: 1197–1213.

52. Johnston AP. Schwann cells: an emerging player in tissue regeneration. *Stem Cell Investig* 2017; **4**: 14.

53. Di Rosa F, Gebhardt T. Bone marrow T cells and the integrated functions of recirculating and tissue-resident memory T cells. *Front Immunol* 2016; **7**: 51.

54. Shan Q, Li X, Chen X, *et al.* Tcf1 and Lef1 provide constant supervision to mature CD8^{+} T cell identity and function by organizing genomic architecture. *Nat Commun* 2021; **12**: 5863.

55. Jung YW, Kim HG, Perry CJ, Kaech SM. CCR7 expression alters memory CD8 T-cell homeostasis by regulating occupancy in IL-7- and IL-15-dependent niches. *Proc Natl Acad Sci USA* 2016; **113**: 8278–8283.

56. Lavaert M, Liang KL, Vandamme N, *et al.* Integrated scRNA-Seq identifies human postnatal thymus seeding progenitors and regulatory dynamics of differentiating immature thymocytes. *Immunity* 2020; **52**: 1088–1104.

57. Rothenberg EV. Single-cell insights into the hematopoietic generation of T-lymphocyte precursors in mouse and human. *Exp Hematol* 2021; **95**: 1–12.

58. Ortinau LC, Wang H, Lei K, *et al.* Identification of functionally distinct Mx1+αSMA+ periosteal skeletal stem cells. *Cell Stem Cell* 2019; **25**: 784–796.

59. Van de Sande B, Flerin C, Davie K, *et al.* A scalable SCENIC workflow for single-cell gene regulatory network analysis. *Nat Protoc* 2020; **15**: 2247–2276.

60. Rao J, Djeffal Y, Chal J, *et al.* Reconstructing human brown fat developmental trajectory *in vitro*. *Dev Cell* 2023; **58**: 2359–2375.

61. Hu Y, Tan LJ, Chen XD, *et al.* Identification of novel potentially pleiotropic variants associated with osteoporosis and obesity using the cFDR method. *J Clin Endocrinol Metab* 2018; **103**: 125–138.

62. Seale P, Bjork B, Yang W, *et al.* PRDM16 controls a brown fat/skeletal muscle switch. *Nature* 2008; **454**: 961–967.

63. Liu H, Zhang C, Zhu S, *et al.* Mohawk promotes the tenogenesis of mesenchymal stem cells through activation of the TGFβ signaling pathway. *Stem Cells* 2015; **33**: 443–455.

64. Rux DR, Song JY, Swinehart IT, *et al.* Regionally restricted Hox function in adult bone marrow multipotent mesenchymal stem/stromal cells. *Dev Cell* 2016; **39**: 653–666.

65. Cartwright T, Perkins ND, L Wilson C. NFKB1: a suppressor of inflammation, ageing and cancer. *FEBS J* 2016; **283**: 1812–1822.

66. Wessells J, Baer M, Young HA, *et al.* BCL-3 and NF-κB p50 attenuate lipopolysaccharide-induced inflammatory responses in macrophages. *J Biol Chem* 2004; **279**: 49995–50003.

67. Hai T, Wolford CC, Chang YS. ATF3, a hub of the cellular adaptive-response network, in the pathogenesis of diseases: is modulation of inflammation a unifying component? *Gene Expr* 2010; **15**: 1–11.

68. Kwon JW, Kwon HK, Shin HJ, Choi YM, Anwar MA, Choi S. Activating transcription factor 3 represses inflammatory responses by binding to the p65 subunit of NF-κB. *Sci Rep* 2015; **5**: 14470.

69. Knights AJ, Yang L, Shah M, *et al.* Kruppel-like factor 3 (KLF3) suppresses NF-κB-driven inflammation in mice. *J Biol Chem* 2020; **295**: 6080–6091.

70. Abe M, Saeki N, Ikeda Y, Ohba S. Kruppel-like factors in skeletal physiology and pathologies. *Int J Mol Sci* 2022; **23**: e15174.

71. Kawata M, Teramura T, Ordoukhanian P, *et al.* Krüppel-like factor-4 and Krüppel-like factor-2 are important regulators of joint tissue cells and protect against tissue destruction and inflammation in osteoarthritis. *Ann Rheum Dis* 2022; **81**: 1179–1188.

72. Choi S, Lee K, Jung H, *et al.* Kruppel-like factor 4 positively regulates autoimmune arthritis in mouse models and rheumatoid arthritis in patients via modulating cell survival and inflammation factors of fibroblast-like synoviocyte. *Front Immunol* 2018; **9**: 1339.

73. Rustenhoven J, Scotter EL, Jansson D, *et al.* An anti-inflammatory role for C/EBPdelta in human brain pericytes. *Sci Rep* 2015; **5**: 12132.

74. Curtis AM, Bellet MM, Sassone-Corsi P, O'Neill LA. Circadian clock proteins and immunity. *Immunity* 2014; **40**: 178–186.

75. Liu H, Zhu Y, Gao Y, *et al.* NR1D1 modulates synovial inflammation and bone destruction in rheumatoid arthritis. *Cell Death Dis* 2020; **11**: 129.

76. Pai P, Sukumar S. HOX genes and the NF-κB pathway: a convergence of developmental biology, inflammation and cancer biology. *Biochim Biophys Acta Rev Cancer* 2020; **1874**: 188450.

77. Morikawa S, Mabuchi Y, Kubota Y, *et al.* Prospective identification, isolation, and systemic transplantation of multipotent mesenchymal stem cells in murine bone marrow. *J Exp Med* 2009; **206**: 2483–2496.

78. Nusspaumer G, Jaiswal S, Barbero A, *et al.* Ontogenic identification and analysis of mesenchymal stromal cell populations during mouse limb and long bone development. *Stem Cell Reports* 2017; **9**: 1124–1138.

79. Ambrosi TH, Sinha R, Steininger HM, *et al.* Distinct skeletal stem cell types orchestrate long bone skeletogenesis. *Elife* 2021; **10**: e66063.

80. Duchamp de Lageneste O, Julien A, Abou-Khalil R, *et al.* Periosteum contains skeletal stem cells with high bone regenerative potential controlled by Periostin. *Nat Commun* 2018; **9**: 773.

81. Lee PY, Wang JX, Parisini E, Dascher CC, Nigrovic PA. Ly6 family proteins in neutrophil biology. *J Leukoc Biol* 2013; **94**: 585–594.

82. Sakaguchi S, Takahashi T, Nishizuka Y. Study on cellular events in post-thymectomy autoimmune oophoritis in mice. II. Requirement of Lyt-1 cells in normal female mice for the prevention of oophoritis. *J Exp Med* 1982; **156**: 1577–1586.

83. Yang S, Fujikado N, Kolodin D, Benoist C, Mathis D. Immune tolerance. Regulatory T cells generated early in life play a distinct role in maintaining self-tolerance. *Science* 2015; **348**: 589–594.

84. Ferreirinha P, Pinheiro RGR, Landry JJM, Alves NL. Identification of fibroblast progenitors in the developing mouse thymus. *Development* 2022; **149**: dev200513.

85. Dhakal M, Miller MM, Zaghouani AA, Sherman MP, Zaghouani H. Neonatal basophils stifle the function of early-life dendritic cells to curtail Th1 immunity in newborn mice. *J Immunol* 2015; **195**: 507–518.

86. Ho NP, Takizawa H. Inflammation regulates haematopoietic stem cells and their niche. *Int J Mol Sci* 2022; **23**: e1125.

87. Houlihan DD, Mabuchi Y, Morikawa S, *et al.* Isolation of mouse mesenchymal stem cells on the basis of expression of Sca-1 and PDGFR-alpha. *Nat Protoc* 2012; **7**: 2103–2111.

88. Hao Y, Hao S, Andersen-Nissen E, *et al.* Integrated analysis of multimodal single-cell data. *Cell* 2021; **184**: 3573–3587.

89. McGinnis CS, Murrow LM, Gartner ZJ. DoubletFinder: doublet detection in single-cell RNA sequencing data using artificial nearest neighbors. *Cell Syst* 2019; **8**: 329–337.

90. Shay DA, Welly RJ, Givan SA, *et al.* Changes in nucleus accumbens gene expression accompany sex-specific suppression of spontaneous physical activity in aromatase knockout mice. *Horm Behav* 2020; **121**: e104719.

SUPPORTING INFORMATION

Additional supporting information may be found online in the Supporting Information section at the end of the article.